

# Effect of Nitrogen Precursors on Lithium Storage Behavior of Nitrogen Doped-Ordered Mesoporous Carbon

*Le Thi Thu Hang*

*Hanoi University of Science and Technology – No. 1, Dai Co Viet Str., Hai Ba Trung, Ha Noi, Viet Nam*

*Received: August 10, 2019; Accepted: June 22, 2020*

## Abstract

Ordered mesoporous carbon (CMK3) before and after doping with nitrogen (N) are prepared successfully by a nanocasting method using sucrose as carbon source, and urea (or melamine) as nitrogen source. After doping N, the materials show an increase in the specific surface area and a slight decrease in the porosity. The N content of the N-doped CMK3 obtained from melamine precursor (CMK3-M) is 5.82 at.%, approximately 4 times as high as that of the N-doped CMK3 obtained from urea precursor (CMK3-U). Among three resultant samples, the CMK3-M exhibits the highest lithium storage capability. Owing to possessing the high N content the CMK3-M can deliver a reversible capacity of 812.7 mAh/g at a current density of 100 mA/g. After 50 cycles of the charge-discharge, the CMK3-M delivers the capacity of 652.06 mAh/g, maintaining 80.2% of its initial reversible capacity with a high coulombic efficiency of 99.5%.

Keywords: Mesoporous carbon, lithium storage, nanocasting

## 1. Introduction

Lithium-ion batteries (LIBs) have been widely used as the power supply of various applications from consumer electronics, transportation vehicles to military apparatus, thanks to their advantages such as superior high energy and power densities, long lifespan, and low self-discharge rate [1]. Especially, the past decade has seen a growing trend towards next-generation LIBs with high charge capacities/power densities developed for electric vehicles, hybrid electric vehicles, aerospace applications, and autonomous electric devices. Meanwhile, conventional LIBs, which are mainly based on Li<sup>+</sup> intercalation/de-intercalation mechanism, have almost reached their limit. This stems from the theoretical capacity of both anode and cathode materials.

Currently, graphite with a theoretical specific capacity of 372 mAh/g has been used as main anode material for LIBs. This specific capacity value seems to be insufficient to meet the increasing energy demand for batteries with higher energy densities, power densities, and rate capabilities [2]. Thus, development of advanced materials having higher reversible capacity, rate capabilities, long-term cyclability and low cost to alter graphite anodes is required. Among them, carbonaceous materials, especially non-graphitic carbon, have emerged as promising alternatives to replace graphite anode for LIBs due to their high electrical conductivity, good hierarchical structure, abundance, and low cost. Moreover, since the lithium storage mechanism of

non-graphitic carbon is somewhat different from that of graphite, these materials show much higher. Particularly, in addition to Li<sup>+</sup> intercalation/de-intercalation mechanism in carbon layers, the non-graphitic carbon materials exhibit lithium adsorption/desorption mechanism on the surface sites of the domain boundary or the grain boundary sites or in nanopores, and cavities [3]. Hence, the surface area and pore size of the carbon materials play an important role in controlling their specific capacity. Besides, chemical doping can be considered as an effective strategy to tailor the electronic and crystalline structures of the carbon materials, enhancing their chemical stability, surface polarity, electric conductivity, and electron-donor properties of non-graphitic carbon. Hence, it has a great impact on LIBs application [4]. Recently, extensive investigations have reported that nitrogen (N) doping can increase the electronic conductivity and rate of electron transfer of carbon materials, for example, carbon nanotube [5], graphene [6], as well as generate more active sites for lithium ion storage.

Since reported in 2001 by Ryoo and workers [7], ordered mesoporous carbon (OMC) materials have been received significant attention owing to their excellent textural characteristics and mesoporous network. This structure provides a highly opened 3D porous host with easy access for guest species, thus facilitating diffusion throughout the pore channels without pore blockage [4]. The outstanding features allow them to be ideal candidates for active materials of LIBs. N-doping into OMCs could be implemented

\* Corresponding author: Tel.: (+84) 973469466  
Email: hang.lenthithu@hust.edu.vn

via three methods as follows: (i) post heat-treatment [8], (ii) chemical treatment [9], and (iii) direct pyrolysis of the N-containing precursors [10]. Among them, only the final method enables gaining a relatively large amount of nitrogen in doped-OMCs, thereby changing the properties of the bulk carbon backbones, particularly the conductivity.

This study reports investigation on the effect of N-containing precursors including urea and melamine on the morphological, structural and physicochemical properties as well as lithium storage behavior of OMC material, namely CMK-3, which serves as anode active material for LIBs.



**Fig. 1.** Schematic diagram of Schematic diagram of synthesis process of N-doped CMK3.

## 2. Experiments

### 2.1. Preparation of ordered mesoporous carbon

Ordered short-rod silica particles (SBA-15) were synthesized via the previously reported process [11, 12]. Ordered mesoporous carbon materials, CMK3, before and after doping nitrogen were prepared by a nano-casting method using SBA-15 as hard template, sucrose as a carbon source [12], urea and melamine as nitrogen source. The CMK3 sample doped nitrogen by using urea precursor is denoted as CMK3-U and the sample prepared from melamine precursor is referred to CMK3-M. The synthesis process is illustrated in Figure 1. In detail, 4 g of SBA-15 was dispersed in an aqueous solution containing 5 g of sucrose, 10 g urea (or melamine) and 0.56 g H<sub>2</sub>SO<sub>4</sub> and then mixed well for 30 mins in an ultrasonic bath. Next, the mixture was dried in an oven at 100 °C for 6 h and at 160 °C for another 12 h.

After treatment in the oven, the obtained dark brown sample was ground prior to re-dispersal in 20 mL of another aqueous solution containing sucrose (3.2 g), 6.2 g urea (or melamine) and H<sub>2</sub>SO<sub>4</sub> (0.36 g) and followed by a drying process at 100 °C for 12 h.

Subsequently, SBA-15 filled by sucrose was carbonized at 900 °C for 5 h in an argon atmosphere to generate the composites of SBA-15 and carbon. To remove the SBA-15 template, SBA-15/carbon composite was soaked in 5wt% HF solution for 48 h. Finally, the products including CMK3, CMK3-U and CMK3-M were centrifuged, washed, and dried at 100 °C under vacuum overnight.

### 2.2. Characterization of morphology, structure and physicochemical properties

The morphology and structure features of the materials were characterized using a field emission scanning electron microscope (SEM, S-4700/EX-200, Hitachi, Japan), a high-resolution X-ray diffractometer (XRD, D/MAX Ultima III, Rigaku, Japan), a X-ray photoelectron spectroscopy instrument (XPS, Multilab 2000, VG, UK), Raman spectrometer (Horiba Jobin-Yvon), and Brunauer-Emmett-Teller (BET) analysis (ASAP 2020, Micromeritics, USA).

### 2.3. Electrochemical characterization

To investigate electrochemical properties of the resultant carbon samples, CR 2032-coin cells were assembled in an argon-filled glove box. A cell was composed of a working electrode, a metallic Li electrode and a glass fiber separator soaked with 100 μL of 1 M LiPF<sub>6</sub> in ethylene carbonate (EC), dimethyl carbonate (DMC) (1:1, by volume), and 5wt% fluoride ethylene carbonate (FEC) as additive.

The working electrode was prepared by mixing well a mixture of 40 mg of CMK3 (or CMK3-U or CMK3-M), 5 mg of super-P carbon, and 5 mg of Polyvinylidene fluoride (PVDF) binder in N-Methyl pyrrolidone (NMP) solvent, then casting on a Cu foil as current collector. After drying in a vacuum oven at 120 °C for 24h, the foil was punched into 14 mm diameter-disks.

Cyclic voltammogram (CV) measurements were carried out using Gamry PC750 potentiostat. The cells were discharged and charged at the potential range of 0.01- 3.0 V vs. Li<sup>+</sup>/Li using an automatic battery cyler (WonATech-WBCS 3000).

## 3. Results and discussion

### 3.1. Morphology and physicochemical properties

Figure 2 presents the SEM and TEM images of the synthesized CMK3 materials. For comparison, the SEM and TEM images of SBA-15 template were included. As shown in the low-resolution SEM images (Figures 2a-d), all the synthesized materials including CMK3, CMK3-U and CMK3-M show the same morphology with that of SBA-15, which was the hard template to create them. These samples were composed of uniform chrysalis-like-short nanorod

particles with  $\sim 1\mu\text{m}$  in length and  $\sim 500\text{ nm}$  in diameter. However, the size of the chrysalis-like particles of the obtained carbon samples seems to be smaller than that of the SBA-15 template. It can be explained that SBA-15 was the hard template, which was used to fill carbon inside. After removal of the outer shell of the SBA-15 template, the three-dimensional (3D) structures of carbon samples were released. This resulted in the smaller size of casted carbon compared with the initial SBA-15 template. Additionally, it is found that after doping N, the morphology of both CMK3-U and CMK3-M samples hardly changed in comparison with CMK3 sample before doping. The nanorods were still interconnected together to form a porous structure. Noticeably, the geometrically structural collapse phenomenon was not observed. Hence, from the low-resolution SEM images, the difference between the morphology of the SBA-15 template and those of the CMK3 carbon materials is hardly identified. In contrast, it is totally clear for observation from the high-resolution SEM and TEM images (Figures 2e-h). Herein, the ordered arrangement of CMK-3 carbon was obviously inferior to its initial template. In addition, more pores left after removal of the SBA-15 template by HF acid were found on the surface of CMK3 nanorods as well.

To confirm whether the structural collapse phenomenon happen inside the nanorods or not, the low angle XRD analysis was conducted within  $2\theta = 0.5\text{-}3.0^\circ$ . As shown in Figure 3a, obviously after etching the SBA-15 template, the sharp diffraction peak of the carbon samples was retained despite a slight shift toward the high diffraction angle. This indicates the integrity of the ordered mesoporous structure of the synthesized carbon samples, which is

in high agreement with the previous reports [8, 9]. From the wide angle XRD analysis in Figure 3b, it is recognized that XRD pattern of the carbon samples is quite different from that of the SBA-15 template, which only possesses a broad peak representing amorphous structure. All the CMK3, CMK3-U and CMK3-M samples exhibit two broad diffraction peaks at  $2\theta = 24^\circ$  and  $2\theta = 44^\circ$ . These peaks correspond to the (002) and (100) diffraction indexes for disordered carbon phase and graphitized carbon, respectively [13], indicating their nature of turbostratic carbon structure.

**Table 1.** Physicochemical analysis data of the synthesized carbon samples.

Parameters	CMK3	CMK3-U	CMK3-M
C (at.%)	94.72	92.38	85.71
O (at.%)	5.28	6.16	8.47
N (at.%)	-	1.46	5.82
$S_{\text{BET}}$ ( $\text{m}^2/\text{g}$ )	1049	1124	1091
$d_p$ (nm)	4.16	3.72	3.87
$V_p$ ( $\text{cm}^3/\text{g}$ )	1.09	1.05	1.06

To verify further the carbon structure of the synthesized samples, their Raman spectra were recorded. Figure 3c depicts Raman spectra of the CMK3, CMK3-U and CMK3-M samples between  $400\text{ cm}^{-1}$  and  $4000\text{ cm}^{-1}$ . As seen, both D band around  $1338\text{ cm}^{-1}$  and G band around  $1590\text{ cm}^{-1}$  are present in the Raman spectra of these samples. The D band is related to structural defects and partially disordered structures of the  $\text{sp}^2$  domains while the G band is associated to the  $E_{2g}$  vibration mode of graphitic  $\text{sp}^2$  carbon domains. This again proves the turbostratic structure of the synthesized carbon samples.

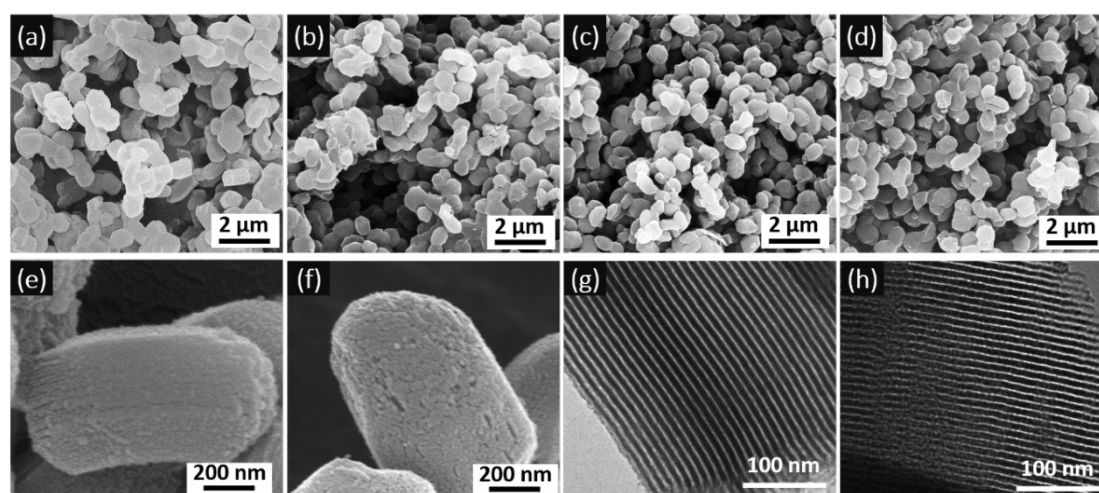


**Fig. 2.** SEM images of (a,e) SBA-15 template, (b,f) CMK3, (c) CMK3-U and (d) CMK3-M; TEM images of (g) SBA-15 and (h) CMK3.

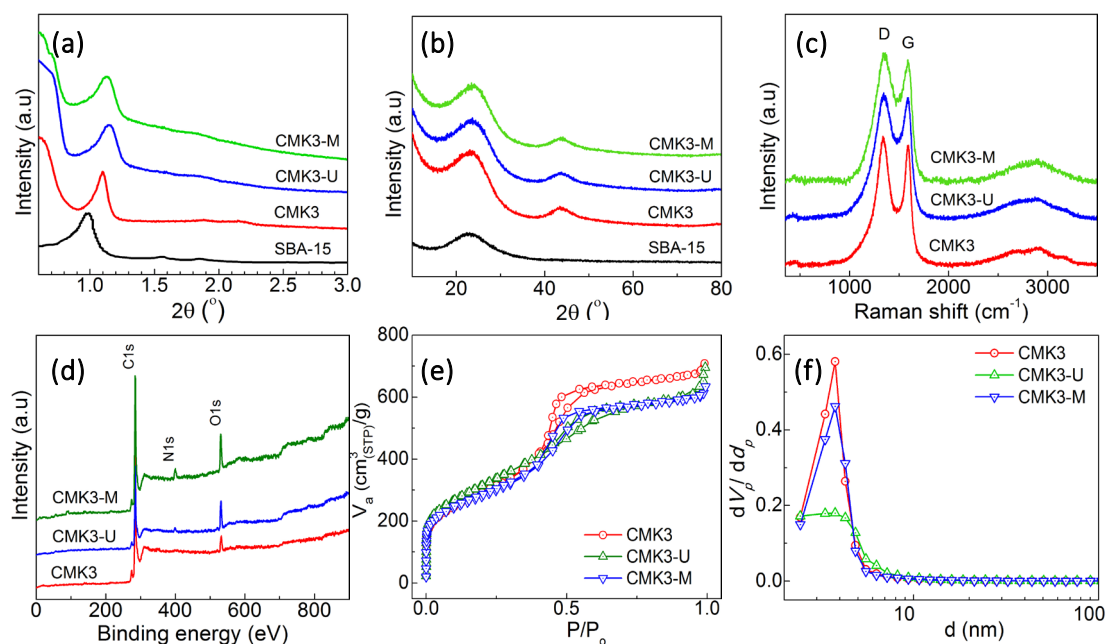


**Fig. 3.** (a) Low and (b) wide angle XRD, (c) Raman spectra, (d) XPS survey spectra, (e)  $\text{N}_2$  adsorption/desorption isotherms, and (f) pore distribution plot of CMK3, CMK3-U and CMK3-M.

XPS is a powerful technique for the characterization of elemental composition and bonding configuration in materials. Figure 3d is XPS survey spectra of the carbon samples. For the XPS spectra of CMK3-U and CMK3-M, the typical peaks of C 1s, O 1s and N 1s were found. In contrast, only two peaks of C 1s and O 1s were detected in the XPS spectrum of CMK3. The presence of N 1s peaks in the CMK3-U and CMK3-M demonstrates the successful incorporation of N in the carbon network of these materials. Their detailed C, O and N contents are listed in Table 1. It can be seen that despite the same mass of the used nitrogen precursors, CMK3-U reveals a lower N content (1.46 at.%) than that of CMK3-M (5.82 at.%). Remarkably, CMK3-M also has a high O content of 8.47 at.% compared with CMK3-U (6.16 at.%), and CMK3 (5.28 at.%). Oxygen is also considered as doped heteroatom and may play as a positive role for lithium storage by increasing defects, disorder, or local electron density around O atoms. Thus, it might offer additional benefit for the CMK3-M material. These XPS results suggest that CMK3-M synthesized from melamine precursor would possess more favorable modified carbon network structure for lithium storage.

From Figure 3e-f, all  $\text{N}_2$  adsorption-desorption isotherms of CMK3, CMK3-U and CMK3-M apparently show a typical hysteresis loop for mesoporous structure materials. This demonstrates that the synthesized CMK3 samples were ordered mesoporous carbon. The textural parameters of these materials are enumerated in Table 1. It is observed that

before doping N the specific surface area ( $S_{\text{BET}}$ ) of CMK3 was  $1049 \text{ m}^2/\text{g}$ . After doping N, the specific surface area of both CMK3-U and CMK3-M increased up to  $1124 \text{ m}^2/\text{g}$  and  $1091 \text{ m}^2/\text{g}$ , respectively. This is ascribed to the activation of carbon from  $\text{NH}_3$  which was generated from decomposition of urea and melamine during the carbonization process of CMK3-U and CMK3-M. Meanwhile, their mean pore size ( $d_p$ ) and total pore volume tended to decrease. However, these changes are negligible.

### 3.2. Electrochemical properties

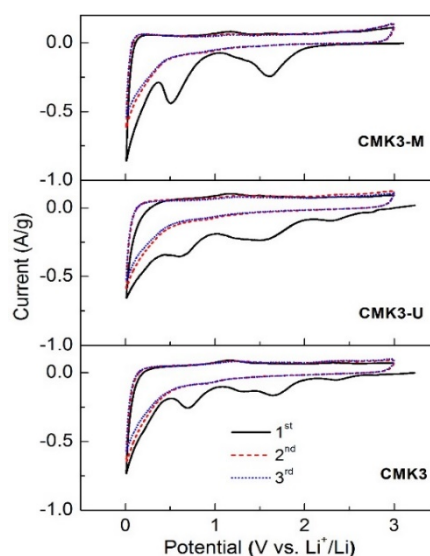


**Fig. 4.** Cyclic voltammograms of CMK3, CMK3-U and CMK3-M electrodes at a scan rate of  $0.1 \text{ mV/s}$  for first three cycles.

To clarify lithium storage mechanism of the CMK3 samples before and after doping N, cyclic voltammetry (CV) measurements were conducted within a potential range from 0.01 to 3.0 V (vs. Li<sup>+</sup>/Li) at a scan rate of 0.1 mV/s with open circuit voltage as initial potential point. Figure 4 shows the CV plots of the CMK3, CMK3-U and CMK3-M electrodes for first three cycles. The CV plots of all electrodes reveal more charge consumption for the reduction process rather than the oxidation process at the first cycle. Moreover, several main cathodic peaks, for example, a peak at ~0.6 V or a peak at 1.6 V, only appeared at this first cycle. From the second cycle onwards, these cathodic peaks totally disappeared, implying the irreversible formation of solid electrolyte interphase (SEI) layer on the surface of the electrodes for the first cycle. In addition, the intensity of these cathodic peaks was found to be higher for the N-doped samples. This implies that the surface functionalization of CMK3-U, and CMK3-M caused by doping N into carbon network promoted the formation of the SEI layer. Also, from the second cycle onwards, the lithium storage process was almost recorded at the potential below 0.45 V, which is contributed by under potential deposition of lithium metal [14]. Another small part contribution to discharge capacity of the electrode came from lithium storage in manifold defects of 3D architectures, pores, cavities, boundaries between differently oriented graphite crystallites in turbostratic carbon, as well as Li binding with heteroatoms [15]. This lithium storage process occurred at the potential above 0.45 V.

For the anodic scan direction, lithium extraction happened within wide potential from 0.01 to 3.0V. It is noted that three weak anodic peaks were observed at around 0.14, 1.18 and 2.4 V. These peaks correspond to lithium extraction from graphite-like nano sized carbon domains, from pore structure/defective sites and from binding with heteroatoms, viz. N atom and O atom, on the surface of the anode materials,

respectively [16-18]. After doping N, both CMK3-U and CMK3-M electrodes showed the higher intensity of the anodic peak at 1.18 and 2.4 V than that of the CMK3 electrode. This resulted in much contribution to the reversible capacity of the electrodes owing to the presence of the heteroatoms in the carbon network.

To elucidate the cyclability of the N-doped CMK3 materials, the electrodes were cycled between the potential from 0.01 V to 3.0 V (vs. Li<sup>+</sup>/Li). Figure 5 illustrates the cycling performance of the CMK3-U and CMK3-M at a current density of 100 mA/g for 50 cycles. As seen in Figure 5a, at the first cycle, the CMK3-M electrode delivered the discharge and charge capacities of 1847.4 and 467.7 mAh/g, respectively. Meanwhile, the CMK3-U and CMK3 electrode only delivered the discharge/charge capacities of 1812.3/762.3 mAh/g and 1576.8/776.6 mAh/g, respectively. The achieved higher capacity of the CMK3-M electrode is attributed to the high content of N heteroatom dopant, which improved electric conductivity [4] as well as generated more defect sites for lithium storage. It is worthy seeing that among three electrodes the CMK3-U electrode revealed the lowest initial coulombic efficiency of 42.1% (Figure 5b). Meanwhile, the rest electrodes showed higher values, 49.3% for CMK3 electrode and 46.9% for CMK3-M electrode. This is due to the highest specific capacity and smallest mean pore size of CMK3-U. Accordingly, the amount of lithium loss caused by formation of irreversible SEI layer and by difficulty in lithium extraction from cavities for the CMK3-U was larger. After 10 cycles of discharge and charge, the previously formed SEI layer became stable. Hence, the specific capacity of the electrodes almost remained stable. After 50 cycles, the CMK3-M could deliver a charge capacity (a reversible capacity) of 652.1 mAh/g, corresponding to a retention of 75% of the initial charge capacity with a coulombic efficiency of 99.5%. At the same time, the CMK3 and CMK3-U

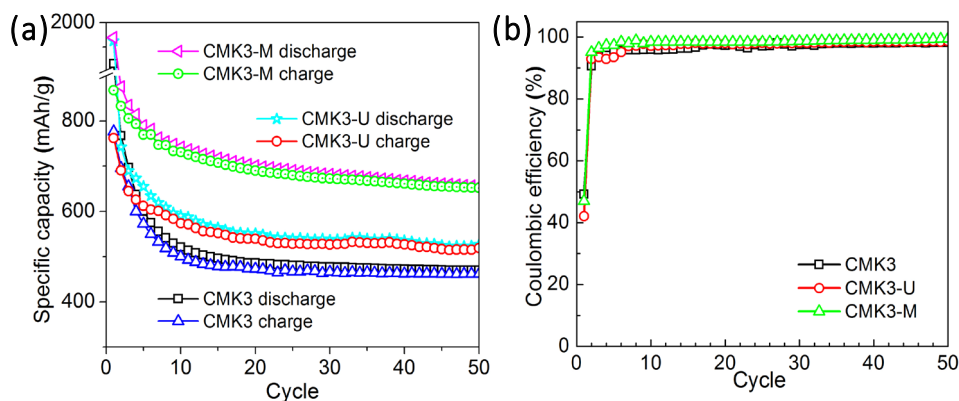


**Fig. 5.** (a) Discharge-charge capacities and (b) coulombic efficiency of CMK3, CMK3-U and CMK3-M electrodes for 50 cycles at a C-rate of 0.1C.

electrodes only delivered a lower reversible capacity of 461.5 mAh/g, and 519.1 mAh/g, respectively. Both these electrodes after 50 cycles showed coulombic efficiencies of 98.2% and 98.6%, which is a little bit lower than that of the CMK3-M electrode.

In brief, the electrodes of CMK3 before and after doping N showed the much higher reversible capacity than that of a commercial graphite anode, with the high coulombic efficiency of > 98%. This proves high potential application of both undoped and N-doped CMK3 as anode active material for LIBs.

#### 4. Conclusion

N-doped CMK3 materials with 3D connected ordered mesoporosity and extremely high specific surface area (> 1000 m<sup>2</sup>/g) have been successfully synthesized by using ordered mesoporous silica as hard-template, sucrose as carbon source and urea as well as melamine as nitrogen source. After doping N, CMK3-M showed the most excellent lithium storage performance for LIBs anode material application with unchanged lithium storage mechanism in comparison with CMK3 mother material. Owing to introducing the N heteroatomic elements into their carbon network, the surface of the materials was modified. The number of defect sites was increased. Besides, the electrical conductivity could be increased. Accordingly, the lithium storage performance of the N-doped CMK3 materials were improved significantly.

#### Acknowledgements

This research was financially supported by the Vietnam Ministry of Education and Training (MOET) through the project with the code B2018-BKA-62.

#### References

- [1]. T. Kim, W. Song, D.-Y. Son, L.K. Ono, Y. Qi, *Journal of Materials Chemistry A*, 7 (2019) 2942-2964.
- [2]. A. Manthiram, J.C. Knight, S.-T. Myung, S.-M. Oh, Y.-K. Sun, *Advanced Energy Materials*, 6 (2016) 1501010.
- [3]. M. Winter, J.O. Besenhard, M.E. Spahr, P. Novák, *Advanced Materials*, 10 (1998) 725-763.
- [4]. H. Chen, F. Sun, J. Wang, W. Li, W. Qiao, L. Ling, D. Long, *Journal of Physical Chemistry C*, 117 (2013) 8318-8328.
- [5]. W.H. Shin, H.M. Jeong, B.G. Kim, J.K. Kang, J.W. Choi, *Nano Letters*, 12 (2012) 2283-2288.
- [6]. H. Xu, L. Ma, Z. Jin, *Journal of Energy Chemistry*, 27 (2018) 146-160.
- [7]. R. Ryoo, S.H. Joo, M. Kruk, M. Jaroniec, *Advanced Materials*, 13 (2001) 677-681.
- [8]. J. Przepiórski, *Journal of Hazardous Materials*, 135 (2006) 453-456.
- [9]. V.C. Almeida, R. Silva, M. Acerce, O.P. Junior, A.L. Cazetta, A.C. Martins, X. Huang, M. Chhowalla, T. Asefa, *Journal of Materials Chemistry A*, 2 (2014) 15181-15190.
- [10]. Z. Qiang, Y. Xia, X. Xia, B.D. Vogt, *Chemistry of Materials*, 29 (2017) 10178-10186.
- [11]. D. Zhao, J. Feng, Q. Huo, N. Melosh, G.H. Fredrickson, B.F. Chmelka, G.D. Stucky, *Science*, 279 (1998) 548.
- [12]. X. Ji, K.T. Lee, L.F. Nazar, *Nature Materials*, 8 (2009) 500.
- [13]. G. Tao, L. Zhang, L. Chen, X. Cui, Z. Hua, M. Wang, J. Wang, Y. Chen, J. Shi, *Carbon*, 86 (2015) 108-117.
- [14]. J.R. Dahn, T. Zheng, Y. Liu, J.S. Xue, *Science*, 270 (1995) 590.
- [15]. J. Hou, C. Cao, F. Idrees, X. Ma, *ACS Nano*, 9 (2015) 2556-2564.
- [16]. F. Su, C.K. Poh, J.S. Chen, G. Xu, D. Wang, Q. Li, J. Lin, X.W. Lou, *Energy & Environmental Science*, 4 (2011) 717-724.
- [17]. B. Guo, X. Wang, P.F. Fulvio, M. Chi, S.M. Mahurin, X.-G. Sun, S. Dai, *Advanced Materials*, 23 (2011) 4661-4666.
- [18]. M. Endo, C. Kim, K. Nishimura, T. Fujino, K. Miyashita, *Carbon*, 38 (2000) 183-197.